Indian J Phys (August 2022) 96(10):2827–2840
https://doi.org/10.1007/s12648-021-02179-x

ORIGINAL PAPER

Stefan blowing on chemically reactive nano-fluid flow containing gyrotactic microorganisms with leading edge accretion (or) ablation and thermal radiation

K Gangadhar[1], K B Lakshmi[2], T Kannan[3] and A J Chamkha[4]*

[1]Department of Mathematics, Acharya Nagarjuna University Campus, Ongole, Andhra Pradesh 523001, India

[2]Department of Mathematics, Lakireddy Balireddy College of Engineering, L.B. Reddy Nagar, Mylavaram, Andhra Pradesh 521230, India

[3]Department of Mathematics, School of Humanities and Sciences, SASTRA Deemed University, Thanjavur, TN, India

[4]Faculty of Engineering, Kuwait College of Science and Engineering, Doha District, Kuwait

Received: 08 April 2021 / Accepted: 29 June 2021 / Published online: 26 July 2021

Abstract: The present study analyzes the forced convective boundary layer flow of viscous incompressible time-established fluid. The base fluid containing water-based nanoparticles and gyrotactic microbes. The flat surface is considered with leading-edge accretion (or) ablation. Characteristics of flow are explored by the impacts of thermal radiation and constructive/destructive chemical reaction. The present flow problem is formed with the partial differential equations, and transformed nonlinear boundary value problems are solved mathematically by the finite difference with the collocation method. There is a good correlation between present work and previous work. Results of selected parameters on velocity, temperature, nanoparticles volume fraction, and microbe density function are discovered. Skin friction, heat transport, mass transfer, and microbes transfer rates are tabular. Efforts of the current work rise in progressive microflow devices to bio-modified nanomaterial dispensation.

Keywords: Nano-fluids; Bioconvection; Stefan blowing; Accretion/ablation; Radiation; Chemical reaction

List of symbols

$\overrightarrow{V_1}$	Velocity vector (ms^{-1})
$\overrightarrow{V_2}$	Average swimming velocity vector of microorganisms $(\mathrm{m}^2\mathrm{s}^{-1})$
(u_1, v_1)	Velocity components (ms^{-1})
(x_1, y_1)	Cartesian coordinates (m)
C_∞	Ambient nanoparticle volume fraction
Cf_{x_1}	Skin friction coefficient
C_w	Wall nanoparticle volume fraction
D_B	Brownian diffusion coefficient
D_T	Thermophoresis diffusion coefficient
D_n	Micoorganism diffusion coefficient
Nn_{x_1}	Local density number of motile microorganisms
Nu_{x_1}	Local Nusselt number
Sh_{x_1}	Local Sherwood number
T_∞	Ambient temperature (K)
T_w	Wall temperature (K)
U_∞	Dimensional ambient velocity (ms^{-1})
W_c	Maximum cell swimming speed (ms^{-1})
$\bar{b}$	Chemotaxis constant (m)
c_p	Specific heat $\left(\mathrm{Jkg}^{-1}\mathrm{K}^{-1}\right)$
$\vec{j}$	Vector flux of microorganisms $\left(\mathrm{kgm}^{-2}\mathrm{s}^{-1}\right)$
k^*	Mean absorption coefficient $(1\mathrm{m}^{-1})$
n_w	Wall motile microorganisms
C	Nanoparticle volume fraction
Kr	Chemical reaction parameter
Lb	Bioconvection Lewis number
Le	Lewis number
Nb	Brownian motion parameter
Nt	Thermophoresis parameter
Pe	Bioconvection Péclet number
Pr	Prandtl number
Rd	Radiation parameter
Re	Reynolds number
T	Nano-fluid temperature (K)
f	Dimensionless stream function
k	Thermal conductivity $\left(\mathrm{Wm}^{-1}\mathrm{K}^{-1}\right)$
n	Number of motile microorganisms
s	Wall mass flux (Stefan blowing)

*Corresponding author, E-mail: a.chamkha@kcst.edu.kw

t Dimensional time (s)

Greek letters

σ^* Stefan Boltzmann constant $\left(\mathrm{Wm^{-2}K^{-4}}\right)$
α Thermal diffusivity $(\mathrm{m^2s^{-1}})$
γ Leading edge accretion/ablation
θ Dimensionless temperature
μ Dynamic viscosity (kg $\mathrm{m^{-1}s^{-1}}$)
ρ Fluid density (kg $\mathrm{m^{-3}}$)
χ Dimensionless number for motile microorganisms
ψ Stream function
ϕ Dimensionless nanoparticles volume fraction

Subscripts

w Condition at wall
∞ Condition in free stream

1. Introduction

Energy sources' consumption has more attention in engineering and technologies due to their importance in the industrial system. Even though it is generally known that the world is facing energy crisis issues due to environmental pollution and global warming, nanotechnology developments are showing the answers to overcome these energy crises. In 1995, Choi [1] works on nano-liquid attracted attention in present years. The nano-liquids work more effectively as coolants in mechanical and engineering areas when compared to others. Nanomaterials are referred as metallic thermophysical parameters absorbed in the base fluid and reinforce their thermal properties. Many efforts have been made to observe the irregular characteristics features of nanoparticles. For example, Buongiorno [2] investigated the 2-point slip procedure, especially Thermophoresis and Brownian movement, to enrich convective heat transport. The flow of nano-fluid along a stretching surface using Buongiorno type is obtainable by Khan and Pop [3]. Current studies about the flow of nano-fluid with various flow characteristics are seen in Refs. [4–25].

A recent analysis on "Bioconvection mostly focus on the enhancing heat transfer and mass transfer with applications in electronics, mechanical, civil process chemical engineering." All other explicitly the cooling frameworks needed for electrical instruments, building protections alongside geothermic atomic garbage removal are high-level bioconvection application areas. Moreover, the research of bioconvection is additionally extended by thermal sinks and heat pipes, reactors. Biological and biotechnological applications of bioconvection are such as blood flow, bio-sensors, micro-enzymes, nano-biotechnology, and bio-medical instrumentation, drug delivery, pharmacokinetics, material detection, and nano-medicine. The transportation of heat transfer inside the material is by convection. I noticed changes in environmental temperatures with cold and hot winds.

Additionally, microbes are likewise considered to be convection in a matter that addresses an impersonate particle's motion in nano-liquids. Generally, unicellular microbes travel haphazardly in a colloidal solution and appear clearly inside a suspension-making density sheet. The natural movement of distinct microorganisms conforming to relative colonial densities is given by the "Bioconvection" phenomenon. The impulsive microorganisms' motions are generally carried out by the explicit inducements that affect the randomized cellular distribution in a colloid. So, microorganisms move because of light, chemicals, oxygen, gravity, density, etc. The motion of microorganisms is called phototaxis, chemotaxis, oxytactic, gyrotactic, gravitactic, etc. The majority of microorganisms show gigantic affectability to the inducement of light; thus, their motions can be constrained by utilizing electromagnetic waves. Hence, bioconvection samples in a colloidal deferment with oxytactic microbes can be constrained by lights. In addition, another stimulation is suppressed to show that different bioconvection samples are either chemotactic or other microorganism preparations. Biofuels are produced by using the bioconvection technique in biotechnology.

Artificial incubation of algae for algal biofuel systems and anaerobic digestion is the key process in biofuel reactors where the motility of microorganisms played a key role. The colonial microorganisms' movement restricted artificially for the light and which tends to the digestion of biomass. Photographs of gyrotactic formation can help to create ideal turbulent stirring during algal development and consistent state light entry with increasing depth of algal development cultures. Secondary, biosensors improvement is one more field; here bioconvection has a potential that can make a quantitative & qualitative location entryway for bio-molecules. Moreover, a biomimetic procedure is additionally evolved to assess provocative and harmful reactions presented by nano-allergens. Kuznetsov [26, 27] examined the identification of continuity in the bioconvection in the presence of oxytactic microbes. Kiari et al. [28] researched some new thermal results in viscous dispersion and thermal conduction in Casson nano-liquid's bioconvective progression to the suction & injection. Nayak et al. [29] described many slip effects in the bioconvective study of non-Newtonian liquid. Magagula et al.[30] investigated the flow of Casson nanomaterial with chemical reaction and nonlinear thermal radiation. Naz [31] deliberate the impact of thermal radiation and stratum on the grade-3 nano-fluid with swimming oxytactic

microorganisms. Khan et al. [32] observed the bioconvection flow of nano-fluid through a Riga surface with nonlinear thermal conduction and activation energy.

At infinity, along with boundary constraints are significant in feigning bioconvective transportation problems. From Stefan's problem [33], blowing impact was invented. For example, in engineering utilizations, paper drying procedure's mass transport is got by evaporation [34]. A turbulent flow of liquid and an additional encouraging flow of the liquids are formed from the concentration of particles [35] for the present work, where the blowing influences the solid's prosaic nature. Also, the blowing is considered due to the flux transport of nanoparticles from the solid surface boundary layer. The concentration of particle transportation varies in the flow field. At the boundary, it is affected by mass blowing, proving that blowing velocity was developed proportional to the mass transfer flux studied by Fang and Jing [33] and Uddin et al. [36], assuming Stefan blowing.

Todd [37] presented a specific rate of accretion or ablation that shows an unstable boundary layer stream model, including the leading edge. This issue creates more attention in current years. Variation in velocity tendencies rises for distinct leading-edge accretion/ablation impacts; hereafter heat, mass, and microbes transfer rates are within the boundary layer. The Buongiorno nano-fluid model with accretion/ablation impacts Rosca and Pop [38] has considered momentum, thermal, and solute boundary layer flows. The problem of unsteady boundary layer flow of nano-fluid containing microorganisms from a plane surface with leading accretion/ablation was scrutinized by Basir et al. [39]. Recently, many studies of computational modeling of fluid flow charactristics have been communicated with diverse applications [40–76]

Encouraged by the above works of literature and applications, this investigater's basic objective is to investigate Stefan's sensitivity to the bioconvective phenomenon of nano-liquid. The liquid is containing oxytactic microbes along a plane surface through the leading edge accretion/ablation. For radiative flux, the nonlinear mathematical equation takes into the heat equation. The second-order chemical reactions are detected in the concentration equation. Still today, no one is stated in the literature with these flow characters. The elaborate nonlinear differential equations system is started mathematically using the finite deference with the colocation method. Thermo-physical quantities of interest are incorporated via graphs and tables. Present work is systematized in the following way. Introduction is given in Sect. 1; mathematical formulation in Sect. 2; numerical approach in Sect. 3; results and discussion in Sect. 4; finally, conclusion in Sect. 5.

2. Mathematical formulation

To enhance the flow model, we consider "An unsteady, two-dimensional, viscous, incompressible laminar forced convective flow of a nano-fluid past a solid stationary semi-infinite plate with leading-edge accretion/ablation." Nano-fluid has oxytactic microbes. Impacts of Stefan blowing, thermal conduction, and biochemical reaction are considered. At a constant surrounding fluid temperature T_∞, a free stream is taken, constant concentration C_∞, and concentration of oxytactic microbes be zero $(n_\infty = 0)$, respectively. Supposed that surface temperature, nanoparticles volume friction, and oxytactic microorganism's density propose are (T_w, C_w, n_w). Boundary layer flow stimulated by bioconvective stag yields in a dilute intermission of nanoparticles; hence volume fraction of nanoparticles is less than 0. 01. The physical formation of the problem is given in Fig. 1. Under the above models and subsequent model, equations are obtained by [26] and [2].

Therefore, following vector field equations are:

$$\nabla \cdot \overrightarrow{V_1} = 0, \tag{1}$$

$$\frac{\partial \overrightarrow{V_1}}{\partial t} + (\overrightarrow{V_1} \cdot \nabla)\overrightarrow{V_1} = -\frac{1}{\rho}\nabla P + \upsilon \nabla^2 \overrightarrow{V_1}, \tag{2}$$

$$\frac{\partial T}{\partial t} + (\overrightarrow{V_1} \cdot \nabla) T = \alpha \nabla^2 T + \tau \left[D_B \nabla T \cdot \nabla C + \left(\frac{D_T}{T_\infty}\right) \nabla T \cdot \nabla T \right], \tag{3}$$

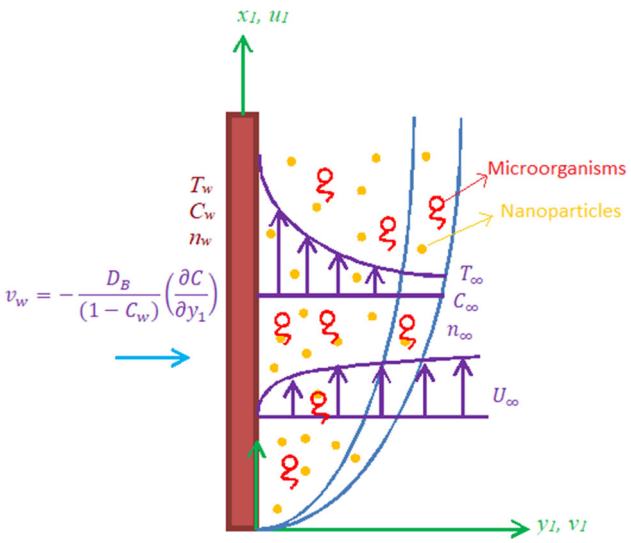

Fig. 1 Flow model and coordinate system

$$\frac{\partial C}{\partial t} + (\overrightarrow{V_1} \cdot \nabla) C = D_B \nabla^2 C + \left(\frac{D_T}{T_\infty}\right) \nabla^2 T - k_0 (C - C_\infty)^2, \tag{4}$$

$$\frac{\partial n}{\partial t} + \nabla \cdot j = 0, \tag{5}$$

here $\nabla = \frac{\partial}{\partial x}\vec{i} + \frac{\partial}{\partial y}\vec{j}, \nabla^2 -$ Laplacian operator, υ-viscosity, ρ-density of the fluid, α-thermal diffusivity, $\tau = (\rho c)_p/(\rho c)_f$-ratio of effective heat and fluid heat capacity of the nanoparticles, D_B-Brownian diffusion coefficient, D_T-thermophoresis diffusion, k_0-chemical reaction rate constant and $\vec{j}$-microorganisms flux defined as:

$$\overrightarrow{j} = n\overrightarrow{V_1} + v\overrightarrow{V_2} - D_n \nabla n, \tag{6}$$

In Eq. (5), D_n-microorganisms diffusion, $\vec{V}_2 = \left(\frac{\bar{b} W_c}{\Delta C}\right) \nabla C$-swimming speed velocity of the microbes, $\bar{b}$-chemotaxis constant and W_c-cell swimming speed at maximum.

Equations (1)–(5) are defined in scalar form:

$$\frac{\partial u_1}{\partial x_1} + \frac{\partial v_1}{\partial y_1} = 0, \tag{7}$$

$$\frac{\partial u_1}{\partial t} + u_1 \frac{\partial u_1}{\partial x_1} + v_1 \frac{\partial u_1}{\partial y_1} = \upsilon \frac{\partial^2 u_1}{\partial y_1^2} + u_e \frac{\partial u_e}{\partial x_1} + \frac{\partial u_e}{\partial t}, \tag{8}$$

$$\frac{\partial T}{\partial t} + u_1 \frac{\partial T}{\partial x_1} + v_1 \frac{\partial T}{\partial y_1} = \alpha \frac{\partial^2 T}{\partial y_1^2} + \tau D_B \frac{\partial T}{\partial y_1}\frac{\partial C}{\partial y_1} + \tau \frac{D_T}{T_\infty}\left(\frac{\partial T}{\partial y_1}\right)^2 - \frac{1}{(\rho c)_f}\frac{\partial q_r}{\partial y_1}, \tag{9}$$

$$\frac{\partial C}{\partial t} + u_1 \frac{\partial C}{\partial x_1} + v_1 \frac{\partial C}{\partial y_1} = D_B \frac{\partial^2 C}{\partial y_1^2} + \frac{D_T}{T_\infty}\frac{\partial^2 T}{\partial y_1^2} - k_0 (C - C_\infty)^2, \tag{10}$$

$$\frac{\partial n}{\partial t} + u_1 \frac{\partial n}{\partial x_1} + v_1 \frac{\partial n}{\partial y_1} + \frac{\bar{b} W_c}{C_w - C_\infty}\left[\frac{\partial}{\partial y_1}\left(n \frac{\partial C}{\partial y_1}\right)\right] = D_n \frac{\partial^2 n}{\partial y_1^2}. \tag{11}$$

Subject to the conditions [36]:

$$u_1 = 0,\ v_1 = -\frac{D_B}{(1 - C_w)}\left(\frac{\partial C}{\partial y_1}\right),\ T = T_w,\ C = C_w,\ n = n_w, \quad \text{as } y_1 = 0, \tag{12}$$

$$u_1 = u_e = U_\infty,\ T \to T_\infty,\ C \to C_\infty,\ n \to 0, \quad \text{as } y_1 \to \infty, \tag{13}$$

here u_e is exterior velocity, υ is kinematic viscosity, ρ is fluid density, and q_r is the radiative heat flux.

By using the Rosseland approximation, the radiative heat flux is [5]

$$q_r = -\frac{4\sigma*}{3k*}\frac{\partial T^4}{\partial y_1}, \tag{14}$$

here $\sigma^* -$ Stefan Boltzmann constant, $k^* -$ mean absorption coefficient. Expand T^4 by applying Taylor's method about T_∞ and ignoring higher-order derivatives, then

$$T^4 \cong 4T_\infty^3 T - 3T_\infty^4. \tag{15}$$

Applying Eq. (15) into Eq. (14), we get

$$\frac{\partial q_r}{\partial y_1} = -\frac{16T_\infty^3 \sigma*}{3k*}\frac{\partial^2 T}{\partial y_1^2}. \tag{16}$$

Use Eq. (16) in Eq. (9), we obtain

$$\frac{\partial T}{\partial t} + u_1 \frac{\partial T}{\partial x_1} + v_1 \frac{\partial T}{\partial y_1} = \alpha \frac{\partial^2 T}{\partial y_1^2} + \tau D_B \frac{\partial T}{\partial y_1}\frac{\partial C}{\partial y_1} + \tau \frac{D_T}{T_\infty}\left(\frac{\partial T}{\partial y_1}\right)^2 + \frac{1}{(\rho c)_f}\frac{16T_\infty^3 \sigma*}{3k*}\frac{\partial^2 T}{\partial y_1^2}. \tag{17}$$

we carry out the changed dimensional stream function, and it contains ablation/accretion impacts at boundary layer edge:

$$\Psi(x_1, y_1, t) = U_\infty \sqrt{\upsilon t \cos\gamma + (\upsilon x_1/U_\infty)\sin\gamma} f(\eta). \tag{18}$$

The coordinate transformation:

$$\eta = y_1/\sqrt{\upsilon t \cos\gamma + (\upsilon x_1/U_\infty)\sin\gamma}. \tag{19}$$

Dimensionless temperature, nanoparticle volume fraction, and density of microorganism functions are defined as follows:

$$\theta(\eta) = (T - T_\infty)/(T_w - T_\infty), \phi(\eta) = (C - C_\infty)/(C_w - C_\infty),\ \chi(\eta) = n/n_w. \tag{20}$$

here η-similarity variable, γ-leading-edge accretion/ablation, t-dimensionless time. Subscripts w and ∞ denotes at a wall and in the free stream. The quantity $(\upsilon t \cos\gamma + (\upsilon x_1/U_\infty)\sin\gamma)$ must be positive [49]. $\Psi(x_1, y_1, t)$ is the streamline function, which are defined as:

$$u_1 = \frac{\partial \Psi}{\partial y_1} \text{ and } v_1 = -\frac{\partial \Psi}{\partial x_1}. \tag{21}$$

Substituting Eqs. (18) and (19) in Eq. (21), we get u_1 and v_1 as:

$$u_1 = U_\infty f', \quad v_1 = \frac{\upsilon}{2}(\eta f' - f)\sin\gamma/\sqrt{\upsilon t \cos\gamma + (\upsilon x_1/U_\infty)\sin\gamma} \tag{22}$$

As per the study, the undeveloped conservation partial differential Eqs. (8), (10), (11), (17) transformed into nonlinear ordinary differential equations as follows:

$$f''' + \frac{1}{2}\sin\gamma f f'' + \frac{1}{2}\cos\gamma \eta f'' = 0, \tag{23}$$

$$\left(1 + \frac{4}{3}Rd\right)\theta'' + \frac{1}{2}\Pr(\eta\cos\gamma + f\sin\gamma)\theta' + Nb\theta'\phi' + Nt\theta'^2 = 0, \tag{24}$$

$$\phi'' + \frac{1}{2}Le\Pr(\eta\cos\gamma + f\sin\gamma)\phi' + \frac{Nt}{Nb}\theta'' - Kr\phi^2 = 0, \tag{25}$$

$$\chi'' + \frac{1}{2}Lb\Pr(\eta\cos\gamma + f\sin\gamma)\chi' - Pe[\chi\phi'' + \chi'\phi'] = 0, \tag{26}$$

The boundary conditions are

$$\begin{aligned} f(0) &= \frac{2}{\Pr Le}\frac{1}{\sin\gamma}s\phi',\ f'(0) = 0,\ \theta(0) = 1,\ \phi(0) = 1,\\ &\chi(0) = 1,\\ f'(\infty) &= 1,\ \theta(\infty) = \phi(\infty) = \chi(\infty) = 0, \end{aligned} \tag{27}$$

here the subsequent dimensionless parameters are: Prandtl number (Pr), Lewis number (Le), Brownian movement parameter (Nb), thermophoresis parameter (Nt), bioconvection Lewis number (Lb), bioconvection Péclet number (Pe), blowing/suction parameter (s), chemical reaction parameter (Kr) and the radiation parameter (Rd). Those parameters are written as:

$$\begin{aligned} \Pr &= \frac{\upsilon}{\alpha},\ \mathrm{Nb} = \frac{\tau D_B(C_w - C_\infty)}{\alpha},\ \mathrm{Le} = \frac{\alpha}{D_B},\\ \mathrm{Nt} &= \frac{\tau D_T(T_w - T_\infty)}{\alpha T_\infty},\\ \mathrm{Lb} &= \frac{\alpha}{D_n},\ \mathrm{Pe} = \frac{\tilde{b}W_c}{D_n},\ s = \frac{(C_w - C_\infty)}{(1 - C_\infty)},\\ \mathrm{Kr} &= \frac{k_0}{U_\infty},\ \mathrm{Rd} = \frac{4\sigma * T_\infty^3}{k * k}. \end{aligned} \tag{28}$$

2.1. Physical quantities

In practical applications, velocity gradient, temperature, nanoparticles concentration &density of microbes is required. Those are in the form of the local coefficient of skin friction Cf_{x_1}, local Nusselt number Nu_{x_1}, local Sherwood number Sh_{x_1}, and local density number of oxytactic microbes Nn_{x_1} are defined as:

$$\begin{aligned} \mathrm{Cf}_{x_1} &= \frac{\mu}{\rho U_\infty^2}\left(\frac{\partial u_1}{\partial y_1}\right)_{y_1=0},\ \mathrm{Nu}_{x_1} = \frac{-x_1}{(T_w - T_\infty)}\left(\frac{\partial T}{\partial y_1}\right)_{y_1=0},\\ \mathrm{Sh}_{x_1} &= \frac{-x_1}{(C_w - C_\infty)}\left(\frac{\partial C}{\partial y_1}\right)_{y_1=0},\ \mathrm{Nn}_{x_1} = \frac{-x_1}{n_w}\left(\frac{\partial n}{\partial y_1}\right)_{y_1=0}. \end{aligned} \tag{29}$$

Employing Eqs. (18)–(22) and (29), the constraints may be re-arranged in the form of similarity variables.

$$\begin{aligned} \mathrm{Re}_{x_1}^{1/2}\mathrm{Cf}_{x_1}\sqrt{\sigma\cos\gamma + \sin\gamma} &= f''(0),\\ \mathrm{Re}_{x_1}^{-1/2}\mathrm{Nu}_{x_1}\sqrt{\sigma\cos\gamma + \sin\gamma} &= -\theta'(0),\\ \mathrm{Re}_{x_1}^{-1/2}\mathrm{Sh}_{x_1}\sqrt{\sigma\cos\gamma + \sin\gamma} &= -\phi'(0),\\ \mathrm{Re}_{x_1}^{-1/2}\mathrm{Nn}_{x_1}\sqrt{\sigma\cos\gamma + \sin\gamma} &= -\chi'(0). \end{aligned} \tag{30}$$

where $\mathrm{Re}_{x_1} = \frac{U_\infty t}{\upsilon}$-local Reynolds number and $\sigma = \frac{U_\infty t}{x_1}$ represents dimensionless time variable, presented by [77].

Note-: In the absence of Eqs. (24)–(26)

1. If $s = 0$ no suction/injection (present model reduces [37]).
2. If $s > 0$ evaporation (particles move from wall to free stream).
3. If $s < 0$ condensations (nanoparticles move from the free stream to the wall).

3. Mathematical method and code authentication

Following Shampine et al. [78], applying the finite difference method mathematically integrates Eqs. (23)–(26) with boundary circumstances of Eq. (27). The FDM uses a collocation method with involuntary grid adaptation to resist the solution's error and convergence. Because the leading equations are cracked in a range domain at infinity condition, the gradients close to the surface are excessive while almost zero at the asymptotic situation. As a result, a dense is needed after the surface, even as an uneven grid is acceptable at infinity conditions. For this reason, the grid model is used to control the computational price and exactness. The Newton approach is used as the generation approach for which a most relative blunders of 10^{-9} as the convergence limit.

One of the vital facets of the current study was selecting an acceptable value of η_∞. The value of η_∞ must be large adequate to take over the asymptotic nature of a solution. Therefore, the solution procedure was started with an initial point of $\eta_\infty = 5$ and then Eqs. (23)–(26) are solved. At that time, the value of η_∞ was enhanced, and $\chi'(0), \phi'(0), \theta'(0)$, as well as $f''(0)$, were observed until the augmentation of η_∞ does not encourage changes in the $\chi'(0), \phi'(0), \theta'(0)$, and $f''(0)$. Through numerical experimentations, it was initiated that $\eta_\infty = 10$ can satisfy the asymptotic boundary

Table 1 Assessment of $f''(0)$ for distinct values of accretion/ablation parameter γ

γ	Rosca and Pop [38]	Todd [37]	Basir et al. [39]	Present study
0	0.56418	0.5642	0.563751	0.564241
$\pi/24$	0.57501	0.5750	0.574585	0.575016
$\pi/12$	0.58072	0.5807	0.580381	0.580729
$\pi/6$	0.57700	0.5770	0.576857	0.577001
$\pi/4$	0.55287	0.5529	0.552780	0.552874
$\pi/3$	0.50721	0.5072	0.507214	0.507218
$5\pi/12$	0.43686	0.4369	0.436849	0.436864
$11\pi/24$	0.38999	0.3900	0.389999	0.389999
$\pi/2$	0.33205	0.3321	0.332051	0.332057

condition in the range of non-dimensional arbitrary constants.

To verify the exactness of the problem, the attained values of $f''(0)$ are correlated with the results of Rosca and Pop [38], Todd [37], and Basir et al. [39] when $s = 0$. The results are potted in Table 1. This table authorizes that there are a good correlation b/w the literature outcomes and present work.

4. Results and discussion

Section 4 is devoted to studying the act of dimensionless flow characters, i.e., temperature profile, velocity profile, nanoparticle volume fraction profile, and microorganisms profiles. In the presence of numerous parameters such as Stefan blowing/suction (s), edge accretion/ablation parameter (γ), Brownian motion (Nb), thermophoresis (Nt), bioconvective Péclet number (Pe), and bioconvective Lewis number (Lb), the present numerical study has been carried out. Moreover, the various leading parameters on Nusselt, Sherwood, and density of oxytactic microbes' numbers are also observed. The numerical outcomes are shown in tables and graphs. For numerical computations, fixed parameters are taken at $\gamma = \frac{\pi}{3}$, $s = 0.2$, $\mathrm{Nt} = 0.1 = \mathrm{Nb}$, $\mathrm{Rd} = 0.2$, $\mathrm{Le} = 5$, $\mathrm{Lb} = 2 = \mathrm{Pe}$, $\mathrm{Kr} = 0.2$, and Prandtl number (Pr) is given as 6.8 except where specified.

Figures 2, 3, 4 and 5 illustrate the impact of Stefan blowing (s) and leading-edge accretion/ablation (γ) on dimensionless velocity, nanoparticle volume fraction, temperature and oxytactic microorganisms' density function profiles. With $-$ ve, Stefan blowing parameter $(s<0)$ dimensionless velocity is enhanced. Generally, with suction at the surface $(s = -1)$, bio-nano-fluid flows over the surface via porous. This restricts the momentum boundary layer by increasing the flow of the boundary layer to the surface. By way of an effect, flow is decreased, leading to an upsurge in momentum boundary layer thickness. By strong blowing $(s = 1)$, hot nano-liquid has exiled the surface where buoyancy forces increased the flow. By enhancing maximum velocity in the boundary layer, this result increases the shearing result. For suction $(s = 1)$ and injection $(s = -1)$, the velocity profiles are distinct. An increase in accretion/ablation impact $(\gamma > 0)$ at the edge shows a reduction in flow, i.e., in velocities. In the case of $(\gamma<0)$, reverse flow with opposite edge accretion is not considered. If $\gamma > 0$ thickness of boundary layer increased with grater suction $(s = -1)$, temperature profile decreases with grater injection $(s = 1)$. With the mass injection, the thermal boundary layer thickness is augmented. If $s = 0$, it corresponds to a solid (impermeable) boundary.

If γ is greater than zero accretion/ablation rate, the temperature profile is strongly heightened, and the thickness of the thermal boundary layer is increased. Comparing thermal field, the velocity field is different from leading-edge accretion/ablation. By strong wall suction $(s = -1)$ throughout the boundary layer, the concentration of nanoparticles diminishes continuously. On the contrary-wise, with stronger blowing $(s = 1)$, nanoparticles concentration is increased. The injection of nano-liquid via the boundary layer boosts nanoparticle diffusion throughout the area, while removing nano-liquid prevents nanoparticle diffusion. Concentration boundary layer thickness increases with increasing blowing, although suction has the reverse impact. Improved accretion/ablation $(\gamma > 0)$ at an edge shows the same impact on the temperature distribution and nanoparticle volume fraction. It improves the nanoparticle concentration and particle size gradually from the boundary to the free stream. Figure 5 shows increases in microorganism density function with greater injection, although strong suction encourages the opposite impact and defeats the density. Microorganisms' transportation is stimulated with blowing via boundary, and thickness of associated boundary layer is raised. Growing accretion/ablation also augments the microorganism density. This study found that the motion of oxytactic microbes is

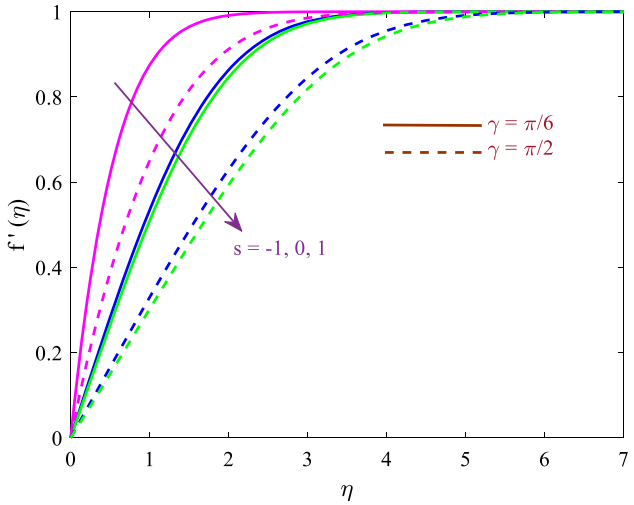

Fig. 2 Variations of $f'(\eta)$ for distinct values of γ and s

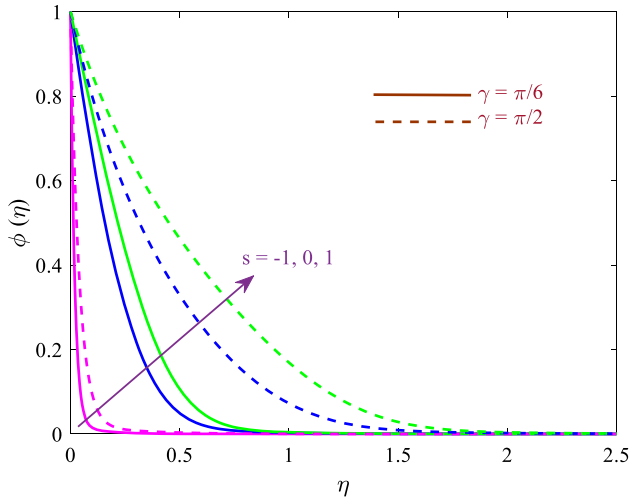

Fig. 4 Variations of $\phi(\eta)$ for distinct values of γ and s

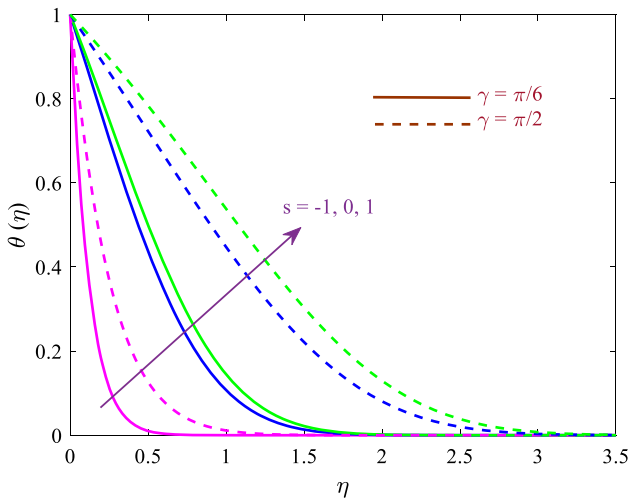

Fig. 3 Variations of $\theta(\eta)$ for distinct values of γ and s

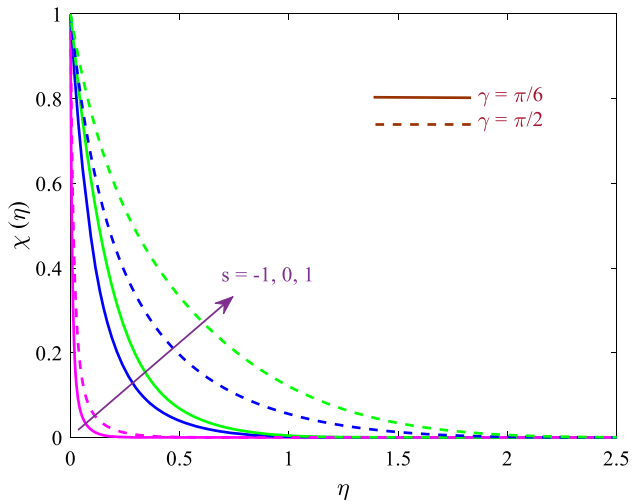

Fig. 5 Variations of $\chi(\eta)$ for distinct values of γ and s

independent of the movement of nanoparticles. The nanoparticles are transported via Brownian motion and by not self-propulsion as with microorganisms.

Figures 6, 7 and 8 represent the temperature distribution, nanoparticles volume fraction and microorganisms, correspondingly, distinct values of Brownian movement parameter (Nb) and suction/blowing parameter (s). Those data, yet again, we assume edge accretion/ablation to be existing with γ given as $\pi/6$. Increment in Brownian movement physically associates with fewer diameter nanoparticles, based on Buongiorno invention working in the present type. For solid boundary case of injection $(s > 0)$, more excellent Nb effects are improved thermal radiation, and this, in turn, upsurges nano-liquid temperatures. On the other hand, lesser Nb values agree to big nanoparticles w, which helps prevent thermal radiation and decline temperatures in nano-fluid and diminish the thermal boundary layer's thickness. An increase in temperatures with lesser nanoparticles results in better heat distribution in nano-fluids related to vorticity. Hereafter, that indicates a decrease in flow with higher Brownian movement impact, though velocity profile has been neglected for brevity.

Figure 7 shows the concentration of nanoparticles repressed with growing Brownian motion parameter. With immense wall suction, both nanoparticles volume fraction & thickness of boundary layer are reduced. The opposite result is shown with wall blowing. Figure 8 shows oxytactic microbe density function reduces with increasing Brownian movement. In addition, with higher wall suction, nano-fluids are uninvolved after the boundary layer region reduces the oxytactic microbe density. With higher wall injection, the flow increases with the oxytactic microbe density values. It is observed that wall injection increases

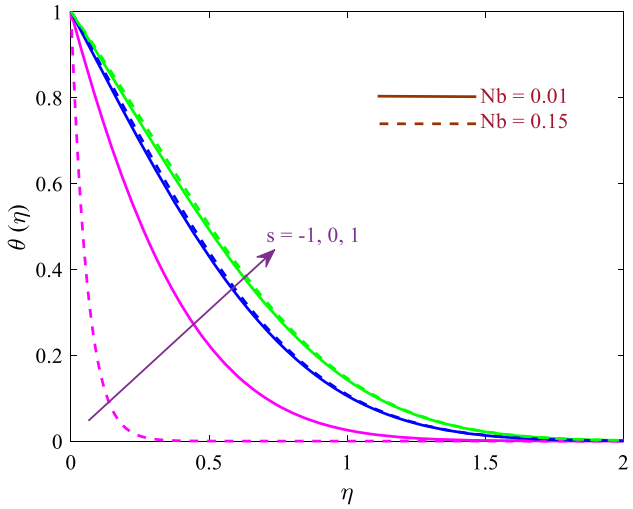

Fig. 6 Variations of $\theta(\eta)$ for distinct values of Nb and s

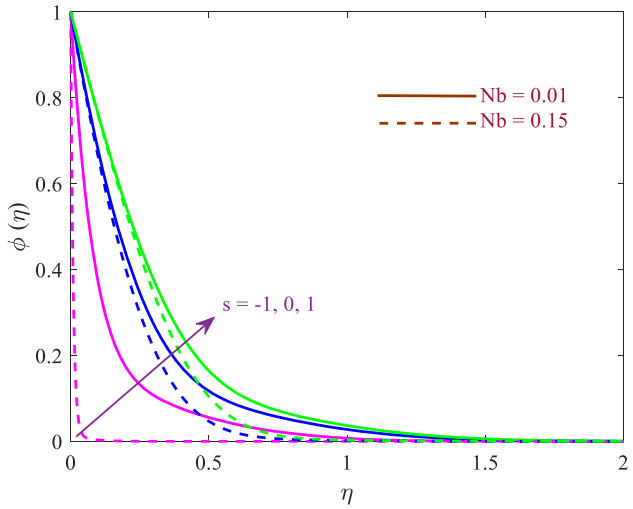

Fig. 7 Variations of $\phi(\eta)$ for distinct values of Nb and s

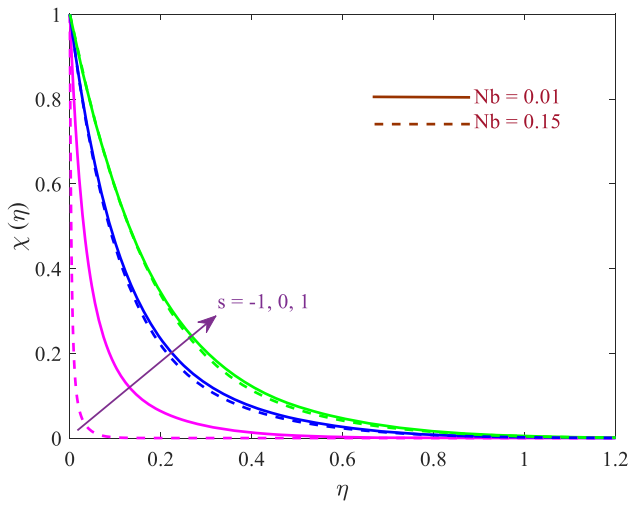

Fig. 8 Variations of $\chi(\eta)$ for distinct values of Nb and s

the concentration of oxytactic microbes in the boundary layer.

Figure 9 depicts the temperature result with joint results of lateral mass flux and thermophoresis parameter (Nt). Progress in Nt also encourages an enhancement in temperature. Thermophoretic movement of nanoparticles boosts thermal distribution in the regime and strengthens the flow. That increases temperatures, i.e., nano-liquid temperature, and enhances & thickness boundary layer. The opposite response is computed for greater suction. From Fig. 10, we observe that thermal distribution increases when increases the radiation parameter (Rd). Physically, one can say that the radiation parameter increases the thermal energy b/w the particles of the fluid. Thus, the temperature increases with the growth of radiation.

Figure 11 displays the result of the convectional Lewis number (Le) on nanoparticle distribution features. Le is the ratio of thermal and concentration nanoparticle diffusion. When Le = 1, the nanoparticles and heat diffusion rates are equal also nanoparticle, and thermal boundary layer thickness will be similar. For Le > 1, thermal diffusion is quicker than nanoparticle types, which decreases the efficacy of nanoparticle migration in nano-liquid. Nanoparticle concentrations are smaller with a bigger Lewis number and strong wall suction present.

Figure 12 displays the effect of the chemical response rate (Kr) on nanoparticle concentration. We observe that + ve approximation of chemical reaction parameter decays concentration and the − ve approximation of chemical reaction parameter enhances the nanoparticles concentration. Thus, the nanoparticle concentration curves decrease the growing chemical reaction parameter. The nanoparticle concentration function's high values are

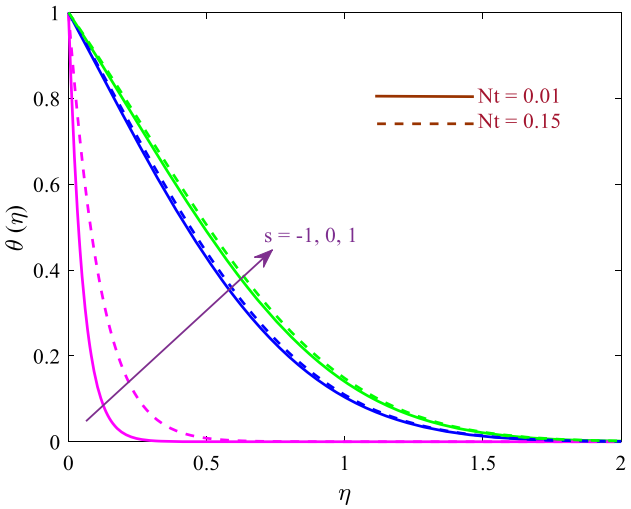

Fig. 9 Variations of $\theta(\eta)$ for distinct values of Nt and s

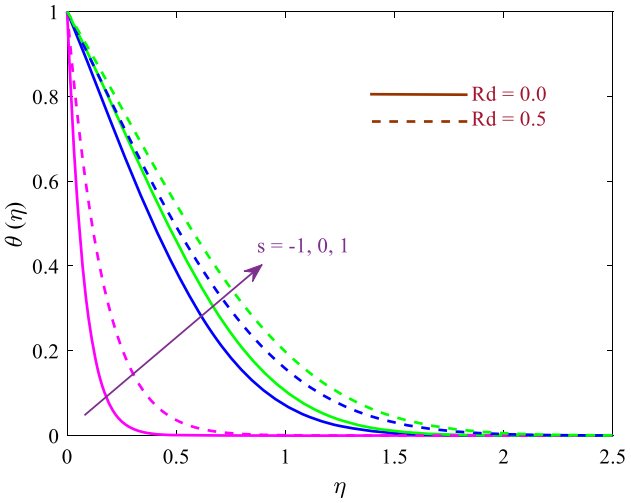

Fig. 10 Variations of $\theta(\eta)$ for distinct values of Rd and s

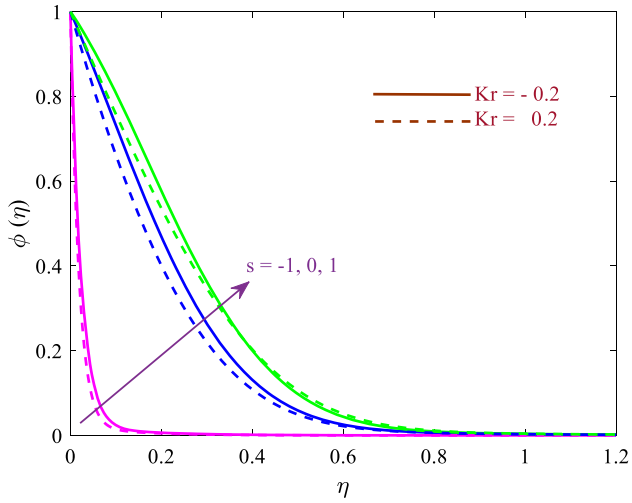

Fig. 12 Variations of $\phi(\eta)$ for distinct values of Kr and s

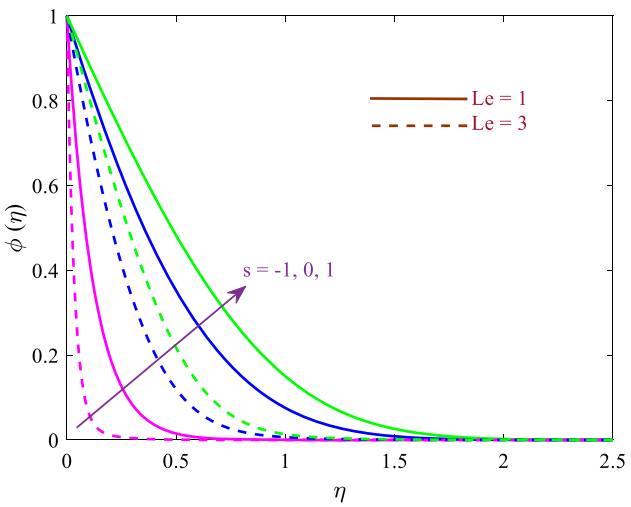

Fig. 11 Variations of $\phi(\eta)$ for distinct values of Le and s

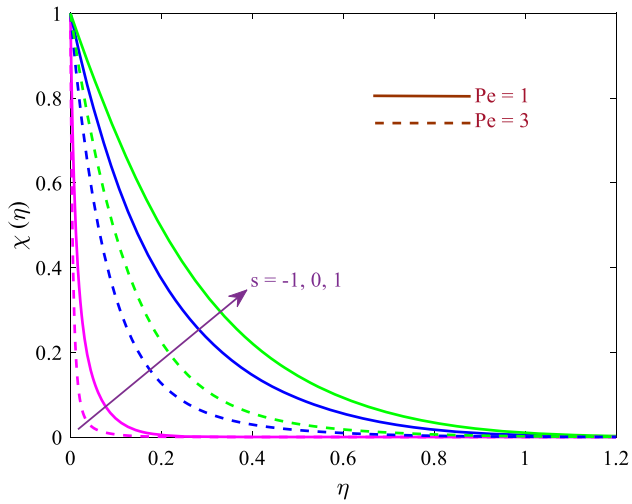

Fig. 13 Variations of $\chi(\eta)$ for distinct values of Pe and s

accomplished with stronger injection, and the smallest sizes correspond to more potent suction at both values of the chemical reaction parameter.

Figure 13 shows the impact of bioconvective Péclet number (Pe) on microbe density. "Bioconvection Péclet number is the ratio of advection and nanoparticles diffusion rate." $\mathrm{Pe} < 10$ is an additional apposite for actual transportation singularities in bioconvective nano-fluid mechanics. Pe features only in the microorganism density conservation Eq. (26) via the coupling terms $-\mathrm{Pe}[\chi\phi'' + \chi'\phi']$, which effectively links the nanoparticle concentration, and microorganism fields. Those relations speciously have a noticeable effect on the growth of density function of microbes. "Bioconvection" is produced from the interior energy of microbes. Microbes boost quicker with greater swimming speed and then, therefore, decrease their convections, i.e., density function. It was exposed that injection can enhance concentration amounts of microbe, while suction may lead to decrease.

Figure 14 shows the result of bioconvective Lewis number (Lb) on microbe density. The number is 5 for the traditional Lewis number, which means the thermal distribution rate is five times the nanoparticle distribution rate. For larger Lb that unity, thermal dispersion rate blows oxytactic microbe diffusion rate. Microbe density is increased with a reduction in bioconvective Lewis number. The force of oxytactic microbes is increased, and much more dispersed through the boundary layer is observed at the rate of microbe diffusivity. Here, we noticed that wall injection continuously reaches greater amounts of microbe density function than wall suction.

Table 2 explains collective properties of edge accretion/ablation (γ) and wall mass flux (s) parameters on wall skin friction. Increasing the leading edge accretion/ablation

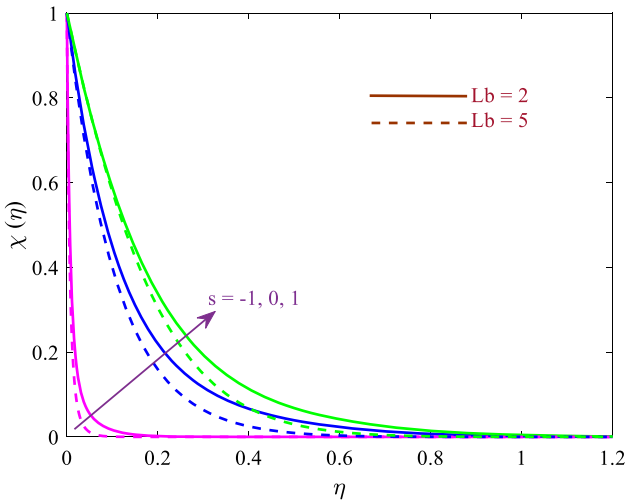

Fig. 14 Variations of $\chi(\eta)$ for distinct values of Lb and s

parameter substantially reduces skin friction for any values of s. But larger values are calculated when wall suction is present $(s<0)$ associated with when wall blowing is present $(s>0)$. The boundary layer is obviously decreased with higher edge accretion/ablation impact $(\gamma>0)$.

Tables 3 and 4 gives reaction in wall heat transport rate with distinct values of leading-edge accretion/ablation parameter (γ), Brownian movement parameter (Nb), thermophoresis parameter (Nt), and wall mass flux parameter (s). Growing edge accretion/ablation powerfully decreases wall heat transport rate both suction and injection. With enhancing the Brownian movement result, nanoparticles are reduced in size. These reduce the heat transport rate to the wall since larger temperatures are encouraged in the liquid body with smaller nanoparticles & thermal energy which is taken in the liquid with lower transport rates to the wall. The reverse impact is deceptive with lower Nb values, which implies more remarkable nanoparticles, smaller temperatures, and larger heat transport rates to the wall. Furthermore, growth in the thermophoresis parameter reduces the heat transport rates to the wall.

Tables 5 and 6 describe the result of leading-edge accretion/ablation parameter (γ), Brownian movement (Nb), the chemical reaction rate (Kr), and wall mass flux (s) on nanoparticle mass transfer rate at the wall. Nanoparticle wall mass transfer rate is pointedly larger with suction $(s<0)$ compared with blowing $(s>0)$, which implies that obliteration of liquid motion inspires nanoparticle distribution at the wall. With higher edge accretion/ablation parameters, nanoparticle wall mass transport rate values are powerfully lessening. In contrast, with an upsurge in Brownian movement and chemical reaction parameters, they are improved.

Tables 7 and 8 give the results of distinct bioconvective parameters (& Pe) on the oxytactic microbe wall mass transport rate, $-\chi'(0)$. Growing bioconvective Lewis number (Lb) meaningfully augments the oxytactic microbe wall mass transport rate regardless of whether injection or suction is present. With enhancing edge accretion/ablation parameter, oxytactic microorganism wall mass transport rate is dejected for the case of wall blowing $(s<0)$ and raised with wall suction $(s>0)$. From these tables, it is noted that higher bioconvective Péclet number produces a significant increase in the microbe wall's oxytactic mass transport rate. At the same time, amounts are decreased with higher values of accretion/ablation parameter.

5. Conclusions

In the present work, "a two-dimensional, unsteady, laminar, incompressible, gyrotactic bioconvection nano-fluid boundary layer flow" is analyzed. The surface is considered as flat with a leading accretion/ablation. Wall mass flux properties are also included in the study through the boundary conditions at the wall. Additionally, thermal radiation and exothermic/endothermic second-order constructive/destructive chemical reactions are executed for the accredited flow simulation. The physical facets of the work are completed for distinct physical constants. The

Table 2 Values of $f''(0)$ when $\mathrm{Pr}=6.8,\ \mathrm{Nt}=\mathrm{Nb}=0.1,\ \mathrm{Rd}=0.2,\ \mathrm{Le}=5,\ \mathrm{Lb}=\mathrm{Pe}=2,\ \mathrm{Kr}=0.2$

γ	$f''(0)$				
	$s=-1$	$s=-0.5$	$s=0$	$s=0.5$	$s=1$
$\pi/6$	1.808037	0.631504	0.577001	0.549056	0.530382
$\pi/4$	1.696883	0.604602	0.552874	0.526107	0.508089
$\pi/3$	1.523862	0.554672	0.507218	0.482269	0.465256
$5\pi/12$	1.278636	0.478519	0.436864	0.414276	0.398485
$11\pi/24$	1.120954	0.428197	0.389999	0.368683	0.353450

Table 3 Values of $-\theta'(0)$ when $\mathrm{Pr} = 6.8,\ \mathrm{Nt} = 0.1,\ \mathrm{Rd} = 0.2,\ \mathrm{Le} = 5,\ \mathrm{Lb} = \mathrm{Pe} = 2,\ \mathrm{Kr} = 0.2$

γ	$-\theta'(0)$					
	$\mathrm{Nb} = 0.1$			$\mathrm{Nb} = 0.15$		
	$s = -1$	$s = 0$	$s = 1$	$s = -1$	$s = 0$	$s = 1$
$\pi/6$	7.686419	1.157452	0.943831	15.298780	1.122550	0.916449
$\pi/4$	7.141543	1.082996	0.880462	14.195559	1.050401	0.855004
$\pi/3$	6.334802	0.963423	0.776984	12.570233	0.934470	0.754589
$5\pi/12$	5.216923	0.789768	0.624246	10.321081	0.766052	0.606303
$11\pi/24$	4.502785	0.675835	0.522386	8.881833	0.655536	0.507376

Table 4 Values of $-\theta'(0)$ when $\mathrm{Pr} = 6.8,\ \mathrm{Nb} = 0.1,\ \mathrm{Rd} = 0.2,\ \mathrm{Le} = 5,\ \mathrm{Lb} = \mathrm{Pe} = 2,\ \mathrm{Kr} = 0.2$

γ	$-\theta'(0)$					
	$\mathrm{Nt} = 0.05$			$\mathrm{Nt} = 0.15$		
	$s = -1$	$s = 0$	$s = 1$	$s = -1$	$s = 0$	$s = 1$
$\pi/6$	9.137936	1.180213	0.963806	7.988067	1.135189	0.923854
$\pi/4$	8.480810	1.104300	0.899120	7.427523	1.062159	0.861816
$\pi/3$	7.513312	0.982384	0.793470	6.593640	0.944880	0.760529
$5\pi/12$	6.176085	0.805321	0.637507	5.435254	0.774558	0.611048
$11\pi/24$	5.322065	0.689153	0.533483	4.694490	0.662813	0.511373

Table 5 Values of $-\theta'(0)$ when $\mathrm{Pr} = 6.8,\ \mathrm{Nt} = 0.1,\ \mathrm{Rd} = 0.2,\ \mathrm{Le} = 5,\ \mathrm{Lb} = \mathrm{Pe} = 2,\ \mathrm{Kr} = 0.2$

γ	$-\theta'(0)$					
	$\mathrm{Nb} = 0.05$			$\mathrm{Nb} = 0.15$		
	$s = -1$	$s = 0$	$s = 1$	$s = -1$	$s = 0$	$s = 1$
$\pi/6$	28.463760	3.744972	2.482454	110.684031	3.759681	2.476643
$\pi/4$	26.502964	3.534708	2.356794	102.695989	3.546096	2.350122
$\pi/3$	23.605746	3.227380	2.175317	90.942147	3.234346	2.167732
$5\pi/12$	19.614010	2.820595	1.942543	74.692151	2.821846	1.934181
$11\pi/24$	17.087017	2.580012	1.811848	64.301719	2.577935	1.803440

Table 6 Values of $-\theta'(0)$ when $\mathrm{Pr} = 6.8,\ \mathrm{Nt} = \mathrm{Nb} = 0.1,\ \mathrm{Rd} = 0.2,\ \mathrm{Le} = 5,\ \mathrm{Lb} = \mathrm{Pe} = 2$

γ	$-\theta'(0)$					
	$\mathrm{Kr} = -0.2$			$\mathrm{Kr} = 0.5$		
	$s = -1$	$s = 0$	$s = 1$	$s = -1$	$s = 0$	$s = 1$
$\pi/6$	42.042179	2.485696	1.552601	58.860882	4.519951	3.089416
$\pi/4$	37.320260	2.160971	1.283431	55.569697	4.347397	2.995569
$\pi/3$	29.860394	1.629790	0.941362	50.827795	4.103835	2.867183
$5\pi/12$	17.385632	0.698082	0.364434	44.554196	3.799674	2.716797
$11\pi/24$	3.614336	− 0.344940	− 0.137527	40.780224	3.631579	2.640421

Table 7 Values of $-\chi'(0)$ when $\mathrm{Pr} = 6.8,\ \mathrm{Nt} = \mathrm{Nb} = 0.1,\ \mathrm{Rd} = 0.2,\ \mathrm{Le} = 5,\ \mathrm{Pe} = 2,\ \mathrm{Kr} = 0.2$

γ	$-\chi'(0)$					
	Lb = 2			Lb = 5		
	$s = -1$	$s = 0$	$s = 1$	$s = -1$	$s = 0$	$s = 1$
$\pi/6$	125.690069	8.363045	5.119324	157.131006	9.166238	4.946588
$\pi/4$	116.747686	7.861437	4.821702	145.949958	8.584352	4.616259
$\pi/3$	103.572437	7.124564	4.385675	129.476543	7.727821	4.129022
$5\pi/12$	85.380119	6.135191	3.805296	106.729875	6.564966	3.463367
$11\pi/24$	73.789974	5.536163	3.458635	92.237727	5.846597	3.049189

Table 8 Values of $-\chi'(0)$ when $\mathrm{Pr} = 6.8,\ \mathrm{Nt} = \mathrm{Nb} = 0.1,\ \mathrm{Rd} = 0.2,\ \mathrm{Le} = 5,\ \mathrm{Lb} = 2,\ \mathrm{Kr} = 0.2$

γ	$-\chi'(0)$					
	Pe = 1			Pe = 3		
	$s = -1$	$s = 0$	$s = 1$	$s = -1$	$s = 0$	$s = 1$
$\pi/6$	73.417622	5.030963	3.129143	177.995198	11.870112	7.290260
$\pi/4$	68.191860	4.714535	2.929854	165.333425	11.173292	6.885112
$\pi/3$	60.491809	4.244983	2.632454	146.678564	10.153147	6.296017
$5\pi/12$	49.858121	3.604660	2.225140	120.920920	8.792178	5.522987
$11\pi/24$	43.082229	3.208491	1.972349	104.511874	7.976156	5.071104

following motivating results are stated from the present work:

1. The boundary layer flow decreases at the leading edge by an upsurge in the accretion/ablation result $(\gamma > 0)$. That is it decreases velocity and skin friction but upsurges the thickness of the momentum boundary layer.
2. The temperature, particle volume fraction, and density function of microbes are augmented with increasing accretion/ablation rate $(\gamma > 0)$, as are the connected boundary layer thickness.
3. With greater wall suction $(s = -1)$, the temperature, nanoparticle volume fraction, microbe's density function a reduced, and with more substantial wall injection $(s = 1), a$ reverse trend follows.
4. With a bigger thermal radiation parameter (Rd), the associated thickness of the thermal boundary layer and temperature are increased.
5. Growth in chemical reaction parameters leads to lower nanoparticles dispersion and its boundary layer thickness.
6. For wall injection $(s<0)$ particles, the wall mass transport rate is decreased and increased for wall suction $(s > 0)$ by increasing the leading-edge accretion/ablation parameter.
7. Through bigger edge accretion/ablation parameters, the nanoparticle wall mass transport rate is repressed and increased with an upsurge in the ordinary Lewis number.
8. Wall heat transport rate is reduced by growing edge accretion/ablation $(\gamma > 0)$ Brownian movement (Nb) and thermophoresis (Nt) parameters.
9. There is a good correlation between numerical results and already published work [37–39].

The current work has considered Newtonian nano-fluids. Further research will discourse non-Newtonian bioconvective nano-fluid flow with space-dependent heat generation due to gravitation and will be discussed in detail. It is assumed that this study will enhance the understanding of flow process dynamics such as that found in various biological and industrial applications.

References:

[1] SUS Choi *In: Proceedings of the ASME international mechanical engineering congress and exposition* FED **231**/MD **66**:99 (1995).
[2] J Buongiorno *J Heat Transf.* **128** 240 (2006).
[3] W A Khan and I Pop *Int. J. Heat Mass Transf.* **53** 2477 (2010).
[4] R Naz, F Mabood, M Sohail and I Tlili *J. Mater. Res. Technol.* **9** 5577 (2020).
[5] M Sohail, R Naz and S I Abdelsalam *Phys. Scr.* **95** 045206 (2020).
[6] M Sohail, R Naz and S I Abdelsalam *Phys. A Stat. Mech. Appl.* **537** 122753 (2020).

[7] R Naz, S Tariq and H Alsulami *Alexandria Eng. J.* **59** 247 (2020).
[8] S M R S Naqvi, T Muhammad and M Asma *Physica A Stat Mech Appl.* **550** 123988 (2020).
[9] M V S Rao, K Gangadhar, A J Chamkha and P Surekha *Arab J Sci Eng.* **46** 2493 (2021).
[10] M Sheikholeslami, A S Mikhail, S Ahmad and T Iskander *Physica A Stat Mech Appl.* **146** 124058 (2020).
[11] H Hanif, I Khan and S Shafie *J. Therm. Anal. Calorim.* **141** 2001–2017 (2020).
[12] I Shahzadi and S Bilal *Comput. Methods Programs Biomed.* **187** 105248 (2020).
[13] M Zufar, P Gunnasegaran, H Kumar and K Ng *Int. J. Heat Mass Transf.* **146** 118887 (2020).
[14] Z Chen, D Zheng and J Wang L Chen and B Sundén *Renew Energy* **147** 1011 (2020).
[15] P Nithya and M Sundrarajan *J. Photochem. Photobiol. B: Biol.* **202** 111706 (2020).
[16] T J Choi, M S Park, S H Kim and S P Jang *Int. J. Heat Mass Transf.* **169** 120903 (2021).
[17] C J Ho, C-Y Cheng, T-F Yang, S Rashidi and W-M Yan *Int. J. Heat Mass Transf.* **169** 120961 (2021).
[18] N Ullah, S Nadeem and A Saleem *J Taiwan Inst Chem Eng.* **113** 428 (2020).
[19] R Harish and R Sivakumar *Int J Mech Sci.* **190** 106033 (2021).
[20] D Kushawaha, S Yadav and D K Singh *Int J Mech Sci.* **191** 106085 (2021).
[21] V YaRudyak, A V Minakov and M I Pryazhnikov *J Mol Liq.* **329** 115517 (2021).
[22] N H Abu-Hamdeh, R A R Bantan, A Golmohammadzadeh and D Toghraie *J Mol Liq.* **325** 115149 (2021).
[23] M Bahiraei and N Mazaheri *Adv Powder Technol.* **32** 211 (2021).
[24] Y Li, Y Zhai, M Ma, Z Xuan and H Wand *Int. Commun. Heat Mass Transf.* **122** 105181 (2021).
[25] M H Esfe, M Bahiraei, A Torabi and M Valadkhani *Int. Commun. Heat Mass Transf.* **120** 104859 (2021).
[26] A V Kuznetsov *Int. Commun. Heat Mass Transf.* **37** 1421 (2020).
[27] A V Kuznetsov *Nanoscale Res. Lett.* **6** 100 (2011).
[28] R R Kairi, S Shaw, S Roy and S Raut *J. Heat Transfer.* **143** 031201 (2021).
[29] M K Nayak, J Prakash, D Tripathi, V S Pandey, S Shaw and O D Makinde *Heat Transfer Asian Res.* **49** 135 (2020).
[30] V M Magagula, S Shaw and R R Kairi *Heat Transfer Asian Res.* **49** 2449 (2020).
[31] R Naz *Int. Commun. Heat Mass Transf.* **117** 104788 (2020).
[32] S U Khan, K Al-Khaled and M Ijaz Khan *Int. Commun. Heat Mass Transf.* **119** 1966 (2020).
[33] T Fang and W Jing *Commun Nonlinear Sci Numer Simul.* **19** 3086 (2014).
[34] G Nellis, S Klein *Cambridge University Press, New York, USA* E**23** (2009).
[35] JH IV Lienhard, JH V Lienhard *3rd edn. Phlogiston Press, Cambridge* 662 (2005).
[36] J Uddin, M N Kabir and O A Beg *Int J Heat Mass Transf.* **95** 116 (2016).
[37] L Todd *Fluid Dyn Res.* **19** 235 (1997).
[38] N C Rosca and I Pop *Comput Fluids.* **95** 49 (2014).
[39] M F M Basir, M J Uddin, O A Beg and A I M Ismail *J Braz. Soc. Mech. Sci. Eng.* **39** 4519 (2017).
[40] Y Menni, A Azzi and A Chamkha *J Therm Anal Calorim* **135** 1951 (2019).
[41] Y Menni, A Azzi and A J Chamkha *J Appl Comput Mech* **4** 375 (2018).
[42] Y Menni, A J Chamkha and A Azzi *Spec Top Rev Porous Media* **9** 1 (2018).
[43] Y Menni, A J Chamkha and A Azzi *J Nanofluids* **8** 893 (2018).
[44] Y Menni et al. *Spec Top Rev Porous Media* **11** 1 (2020).
[45] Y Menni et al. *MMEP* **6** 415 (2019).
[46] N Sakhri, Y Menni, A J Chamkha, M Salmi and H Ameur *J Eng Sci* **64** 83 (2020).
[47] Y Menni, A J Chamkha, C Zidani and B Benyoucef *Int J Numer Method H* **30** 3027 (2020).
[48] Y Menni, A J Chamkha, A Azzi, C Zidani and B Benyoucef *MMEP* **6** 77 (2019).
[49] Y Menni, A Azzi and A J Chamkha *J New Technol Mater* **8** 58 (2018).
[50] Y Menni, A Azzi and A J Chamkha *Period Polytech Mech Eng* **62** 209 (2018).
[51] Y Menni, A Azzi and A J Chamkha *Defect Diffus Forum* **388** 378 (2018).
[52] Y Menni, A Azzi, A J Chamkha and S Harmand *Int J Numer Method H* **29** 3908 (2019).
[53] Y Menni, A Azzi, A J Chamkha and S Harmand *J Appl Comput Mech* **5** 231 (2019).
[54] Y Menni, A Azzi and A J Chamkha *J Mech Eng Sci* **12** 3888 (2018).
[55] Y Menni, A Azzi and A J Chamkha *J Appl Comput Mech* **5** 616 (2019).
[56] Y Menni, A Azzi and A J Chamkha *Int J Numer Method H* **29** 1815 (2019).
[57] Y Menni, A J Chamkha and A Azzi *J Appl Comput Mech* **6** 741 (2020).
[58] Y Menni, A J Chamkha, G Lorenzini and B Benyoucef *MMEP* **6** 170 (2019).
[59] Y Menni, A J Chamkha, C Zidani and B Benyoucef *Period Polytech Mech Eng* **63** 100 (2019).
[60] N Sakhri, Y Menni and A J Chamkha *J Appl Comput Mech* (2020). https://doi.org/10.22055/JACM.2020.31237.1843
[61] Y Menni, A J Chamkha, C Zidani and B Benyoucef *MMEP* **6** 52 (2019).
[62] Y Menni, G Lorenzini, R Kumar, B Mosavati and S Nekoonam *Math Probl Eng* **2021** 1 (2021).
[63] Y Menni, A Azzi and A J Chamkha *Heat Trans Res* **50** 1781 (2019).
[64] Y Menni, A J Chamkha, A Azzi and C Zidani *Int J Fluid Mech Res* **47** 23 (2020).
[65] A J Chamkha and Y Menni *MMEP* **7** 178 (2020).
[66] Y Menni, A J Chamkha and O D Makinde *Defect Diffus Forum* **401** 117 (2020).
[67] Y Menni, A J Chamkha, C Zidani and B Benyoucef *MMEP* **6** 21 (2019).
[68] Y Menni, A J Chamkha, C Zidani and B Benyoucef *Arch Thermodyn* **41** 33 (2020).
[69] Y Menni, H Ameur, A J Chamkha, M Inc and B Almohsen *Therm Sci* **24** 267 (2020).
[70] Y Menni et al. *Numer Heat Transfer Part A Appl* **79** 311 (2021).
[71] M Salmi, Y Menni, A J Chamkha, H Ameur, R Maouedj and A Youcef *Comput Model Eng Sci* **126** 147 (2021).
[72] C J Ho, Y-C Liu, M Ghalambaz and W-M Yan *Int J Heat Mass Transf* **155** 119858 (2020).
[73] M Ghalambaz and J Zhang *Int J Heat Mass Transf* **146** 118832 (2020).
[74] S A M Mehryan, M Ghalambaz, L S Gargari, A Hajjar and M Sheremet *J Energy Storage* **28** 101236 (2020).
[75] M Ghalambaz, S A M Mehryan, A Hajjar and A Veismoradi *Adv Powder Technol* **31** 954 (2020).
[76] M Ghalambaz, S M H Zadeh, S A M Mehryan, I Pop and D Wen *Appl Math Model* **77** 1936 (2020).
[77] K Stewartson *Math Proc Camb Philos Soc.* **51** 202 (2008).

[78] LF Shampine, J Kierzenka and MV Reichelt *Tutorial Notes* 1 (2000).